DISCLAIMER

This report was prepared as an account of work sponsored by an agency of the United States Government. Neither the United States Government nor any agency thereof, nor any of their employees, makes any warranty, express or implied, or assumes any legal liability or responsibility for the accuracy, completeness, or usefulness of any information, apparatus, product, or process disclosed, or represents that its use would not infringe privately owned rights. Reference herein to any specific commercial product, process, or service by trade name, trademark, manufacturer, or otherwise does not necessarily constitute or imply its endorsement, recommendation, or favoring by the United States Government or any agency thereof. The views and opinions of authors expressed herein do not necessarily state or reflect those of the United States Government or any agency thereof. Reference herein to any social initiative (including but not limited to Diversity, Equity, and Inclusion (DEI); Community Benefits Plans (CBP); Justice 40; etc.) is made by the Author independent of any current requirement by the United States Government and does not constitute or imply endorsement, recommendation, or support by the United States Government or any agency thereof.

Pacific Northwest
NATIONAL LABORATORY

PNNL-37208

Fully Recyclable CFRP Particles (CRADA 519)

December 2024

Kevin L. Simmons
Yao Qiao
Jose L. Ramos
Daniel R. Merkel
Wenbin Kuang

U.S. DEPARTMENT OF ENERGY

Prepared for the U.S. Department of Energy
under Contract DE-AC05-76RL01830

NOTICE

Printed in the United States of America

Available to DOE and DOE contractors from the Office of Scientific and Technical Information, P.O. Box 62, Oak Ridge, TN 37831-0062
www.osti.gov
ph: (865) 576-8401
fox: (865) 576-5728
email: reports@osti.gov

Available to the public from the National Technical Information Service
5301 Shawnee Rd., Alexandria, VA 22312 ph: (800) 553-NTIS (6847)
or (703) 605-6000
email: info@ntis.gov
Online ordering: http://www.ntis.gov

PNNL-37208

Fully Recyclable CFRP Particles (CRADA 519)

December 2024

Kevin L. Simmons
Yao Qiao
Jose L. Ramos
Daniel R. Merkel
Wenbin Kuang

Prepared for the U.S. Department of Energy under Contract DE-AC05-76RL01830

Pacific Northwest National Laboratory
Richland, Washington 99354

Cooperative Research and Development Agreement (CRADA) Final Report

Report Date: December 2024

In accordance with Requirements set forth in the terms of the CRADA, this document is the CRADA Final Report, including a list of Subject Inventions, to be provided to PNNL Information Release who will forward to the DOE Office of Scientific and Technical Information as part of the commitment to the public to demonstrate results of federally funded research. **PNNL acknowledges that the CRADA parties have been involved in the preparation of the report or reviewed the report.**

Parties to the Agreement:

Battelle as Operator of Pacific Northwest National Laboratory ("PNNL")

CRADA number: 519

CRADA Title: Fully Recyclable CFRP Particles

Responsible Technical Contact at DOE Lab(PNNL):

Kevin L. Simmons (kl.simmons@pnnl.gov)

Yao Qiao (yao.qiao@pnnl.gov)

Name and Email Address of POC at Partner Company(ies):

Technical: Gabriel Iftime (giftime@parc.com)

Technical: Austin Wei (jawei@parc.com)

Business: Mary Kelly (mkelly@parc.com)

Sponsoring DOE Program Office(s): Office of Energy Efficiency and Renewable Energy

Joint Work Statement Funding Table showing DOE funding commitment:

	Funding Amounts			
CRADA Parties	**DOE Funding**	**Funds-In**	***In-kind**	**Total**
Participant(s)	N/A	N/A	$500,000	$500,000
DOE Funding to PNNL	$500,000	N/A	N/A	$500,000
Total of all Contributions	$500,000	N/A	$500,000	$1000,000

Provide a list of publications, conference papers, or other public releases of results, developed under this CRADA:

No publications, conference papers, or other public releases of results, developed under this CRADA:

Provide a detailed list of all subject inventions, to include patent applications, copyrights, and trademarks:

No subject inventions were generated under this CRADA.

Abstract

The proposed resin-enhanced materials, which utilize fully recycled CFRP (carbon-fiber-reinforced polymer) particles, are enabled by PARC's proprietary Chemically Linked Particles Networks (13 granted patents and patent applications) (e.g., [1]). PNNL and PARC have collaborated to develop manufacturing methods, such as vacuum-assisted wet compression molding and filament winding, for fabricating fiber-reinforced composites with the PARC matrix.

PNNL has conducted various mechanical, physical, and thermal characterizations to compare their differences between the composites with baseline and PARC matrices. Those characterizations include density, void volume fraction, optical micrography, uniaxial tension, four-point bending/flexure, interlaminar shear, coefficient of thermal expansion, glass transition temperature, and curing kinetics.

1. Introduction

PNNL and PARC have collaborated to develop advanced manufacturing processes, including wet compression molding and filament winding, that integrate recycled CFRP particles with surface modification techniques in the production of new CFRP parts, as illustrated in Figure 1. A range of properties have been characterized to evaluate the impact of adding recycled CFRP particles to fiber-reinforced composites, demonstrating their effects on the material performance.

This collaboration aims to offer automotive manufacturers an innovative and scalable solution designed to significantly reduce production costs, enhance material performance, and expedite the widespread adoption of CFRP materials across various vehicle classes. By utilizing recycled CFRP particles, which are processed and modified to improve chemical bonding with the matrix, the project seeks to create a more sustainable and cost-effective approach to producing high-performance CFRP components, ultimately benefiting both the automotive industry and the environment.

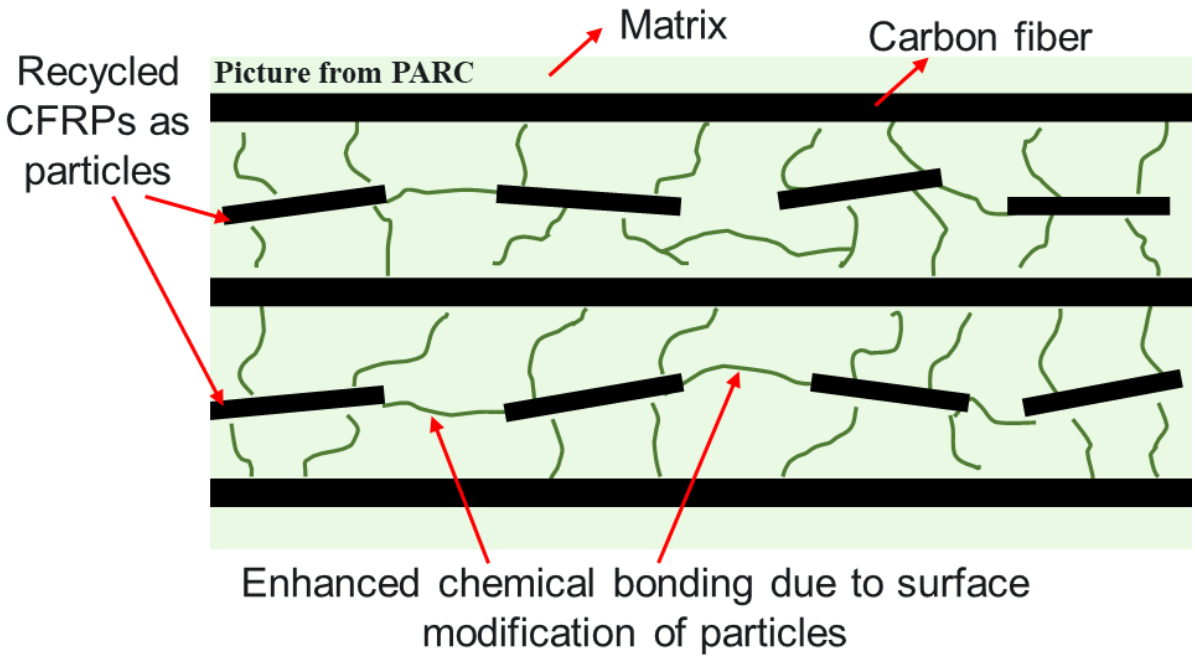

Figure 1. Recycled CFRP particles added to fiber-reinforced composites, with surface modification performed to enhance chemical bonding with the matrix.

2. Materials and Preparation

2.1. Materials

For the baseline matrix, 5 grams of EPON 826, 0.16 grams of 2-Ethyl-4-methylimidazole, and 0.8 grams of DCH-99 hardener were measured and combined. In contrast, for the matrix containing recycled CFRP particles (PARC), 5 grams of EPON 826, 0.136 grams of 2-Ethyl-4-methylimidazole, and 0.68 grams of DCH-99 hardener were measured and combined. In addition, Toray T300 plain weave carbon fabrics were used to fabricate fiber composites.

2.2. Wet Compression Molding

Fiber-reinforced composites were fabricated using the traditional wet compression molding (WCM) method. The process involved the following steps: (1) mixing the matrix for 1.5 minutes at 1200 rpm, followed by degassing for 1.5 minutes at 1700 rpm, and then repeating both steps; (2) preheating the steel mold to 60°C simultaneously; (3) pouring half of the matrix into the mold, placing eight plies of carbon fabrics, and then pouring the remaining matrix into the mold; and (4) closing the mold and curing it at 150°C for 15 minutes.

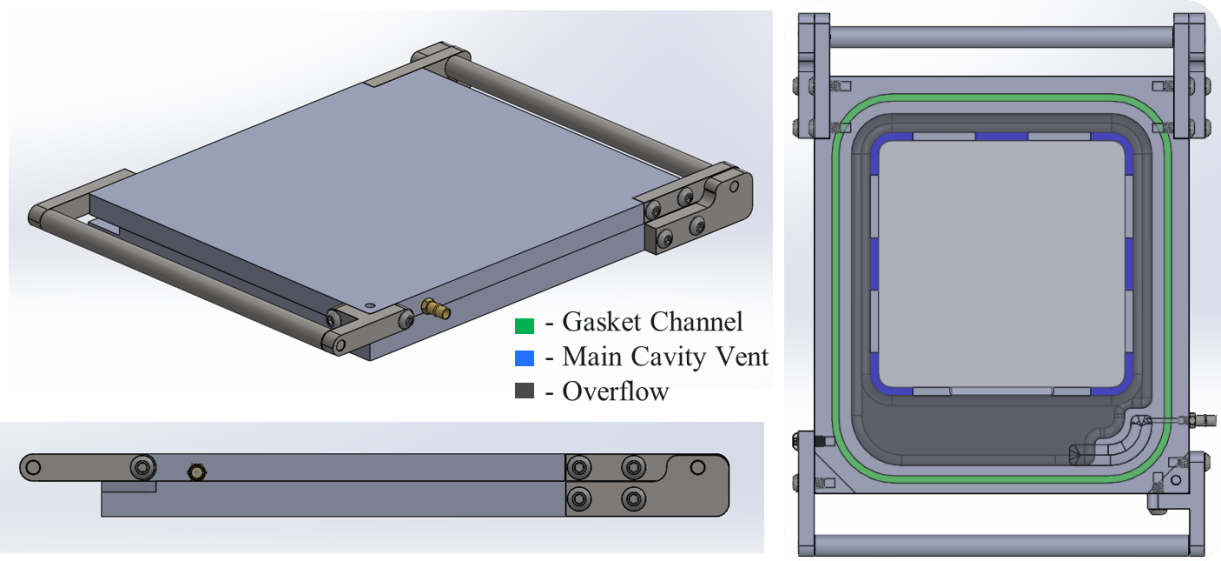

Figure 2. Steel mold for vacuum-assisted WCM to fabricate fiber-reinforced composites.

In addition, an improved method utilizing vacuum-assisted WCM, as shown in Figures 2-3, was employed to fabricate fiber-reinforced composites and compare with the ones fabricated using traditional WCM method. The key difference is the application of a 50 kPa vacuum during the early stage of matrix curing, which helps mitigate air voids trapped in the matrix. All other fabrication steps remain the same as those described for the traditional WCM method.

It is worth noting that various fabrication parameters, including mold preheating time and temperature, composite post-curing time and temperature, as well as matrix mixing and degassing time and speed, were also investigated to optimize the mechanical performance of the composites.

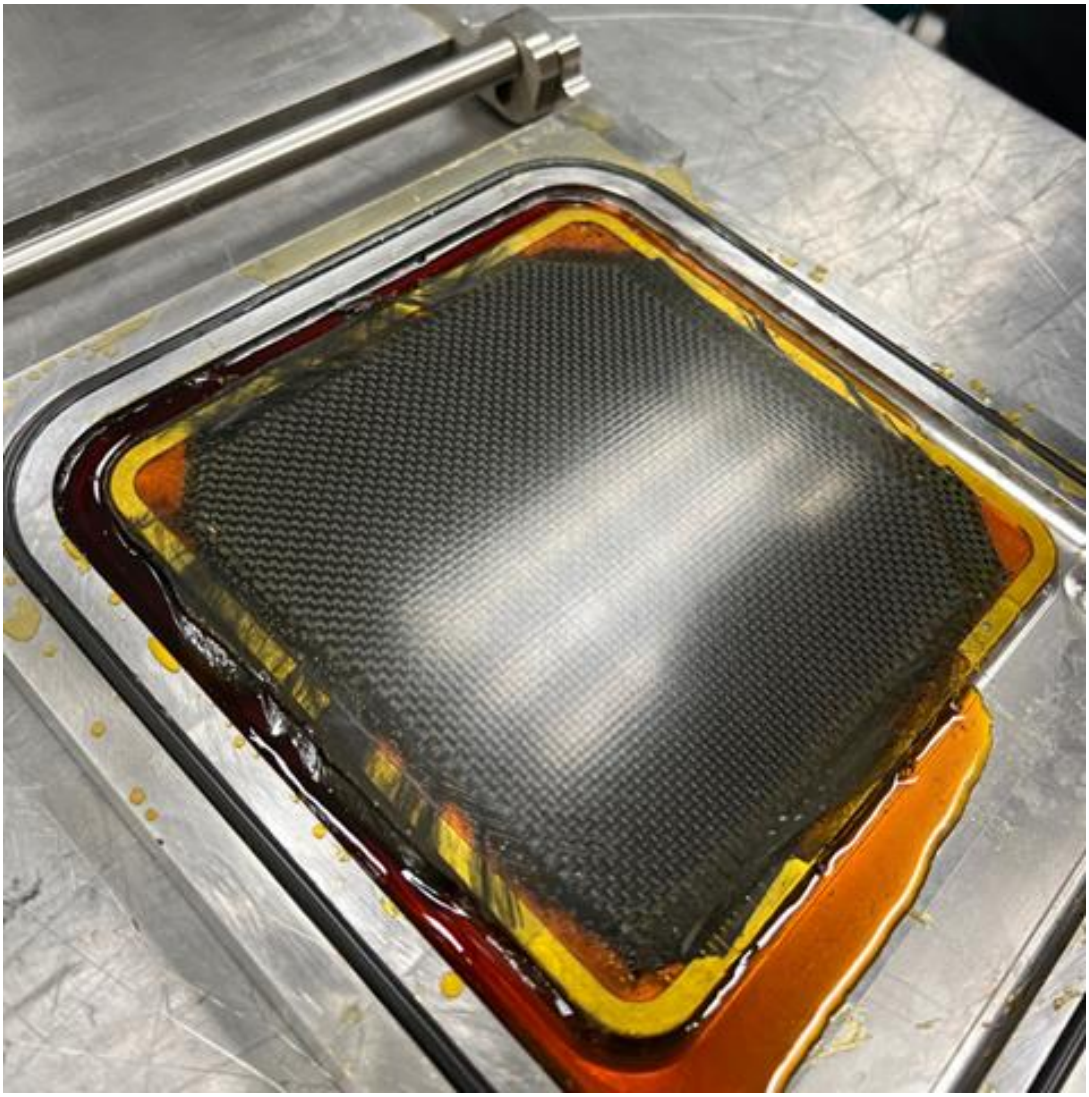

Figure 3. Fiber-reinforced composites fabricated by vacuum-assisted WCM method.

2.3. Filament Winding

Wet filament winding was additionally used to fabricate fiber-reinforced composite rings. The purpose of this fabrication was to measure the interlaminar shear properties of curved composites, representing a slice of a composite vessel. Hexcel AS4 uni-directional carbon fibers were used and wound on an aluminum mold using a filament winder (X-winder) as illustrated in Figure 4. The winding speed was set to 2 rpm, and the number of windings applied was 64.

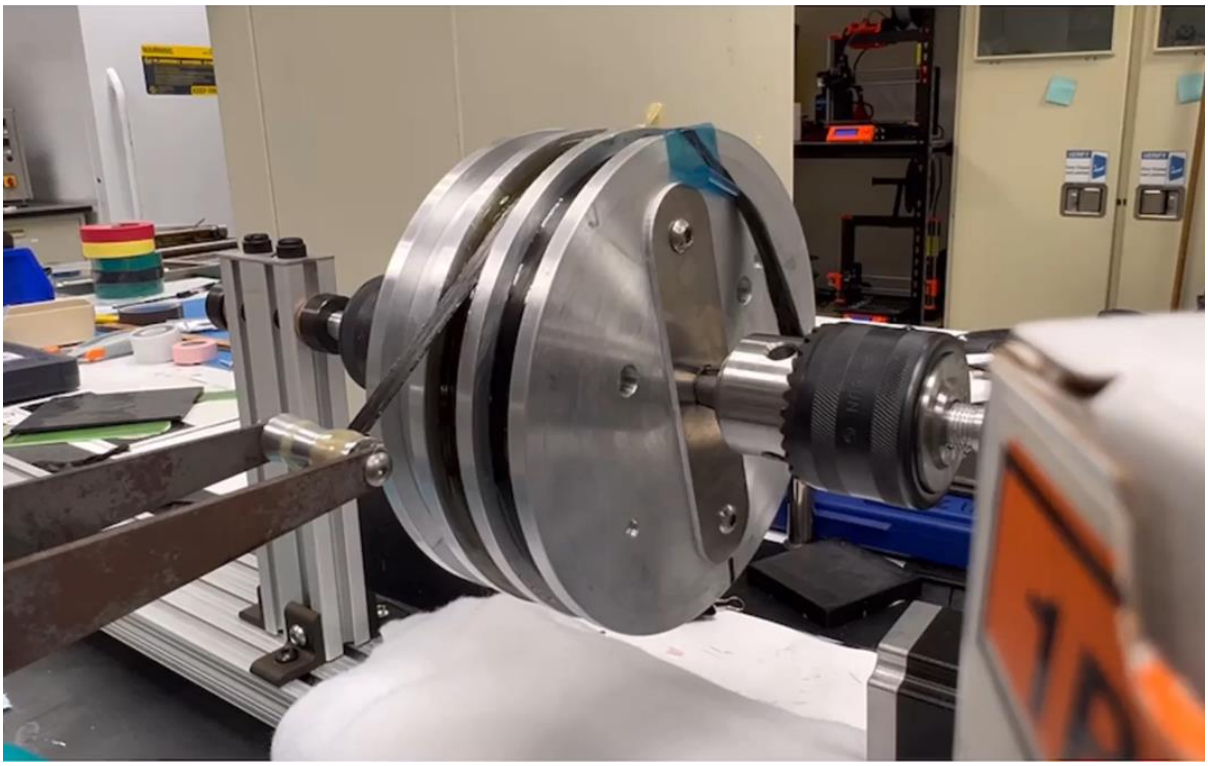

Figure 4. Wet filament winding of fiber-reinforced composite rings.

2.3. Thermal and Mechanical Characterizations

Thermal properties of PARC, including thermal expansion (CTE), glass transition temperature (T_g), and curing kinetics, were initially characterized to compare with those of the baseline matrix. Q800 DMA (Dynamic Mechanical Analyzer) from TA instruments was used to measure the values of CTE and T_g, A static load of 0.001 N and a heating rate of 2 K/minute were applied on a cylindrical matrix. Differential Scanning Calorimetry (DSC) from Mettler Toledo was used to characterize the curing kinetics of the matrix through dynamic heating with three different heating rates (5, 10, and 30 K/minute).

Regarding mechanical testing, three types of tests were conducted in this work: (1) uniaxial tension following ASTM D3039, (2) four-point bending/flexure following ASTM D7264, and (3) short-beam shear following ASTM D2344. An example of testing setup for short-beam shear is illustrated in Figure 5. For uni-axial tension, the rectangular specimen has the dimension of 8 mm x 115 mm x 2.5 mm. The gauge length is approximately 60 mm. For four-point bending/flexure, the rectangular specimen has the dimension of 12 mm x 135 mm x 2.5 mm. The load span was 64 mm, and the support span was 128 mm. For short-beam shear, the specimens were cut from filament-wound composite rings, featured 22-degree segment radius, and had the thickness of approximately 7 mm. All the mechanical tests were performed using an electromechanical Instron 5582 load frame under displacement control with a displacement rate of 1.27 mm/minute. In addition, all composite specimens were painted white and then speckled with black paint to enable Digital Image Correlation (DIC) using Correlated Solutions for quantifying strain fields on the specimen surfaces.

Figure 5. Short-beam shear testing setup for curved fiber-reinforced composites.

2.4. Density and Porosity/Void Characterization

All composites fabricated using WCM and filament winding were cut into pieces with approximate dimensions of 10 mm × 10 mm for density and porosity measurements in accordance with ASTM D792. The densities of all composites were approximately 1.4 g/cm³. For porosity, the baseline composite fabricated using either the traditional or vacuum-assisted WCM method exhibited values ranging from ~1.2% to ~1.4%, while the composite with the PARC matrix had higher porosity, ranging from ~2.1% to ~2.4%. Similarly, the baseline composite fabricated using filament winding showed porosity values ranging from ~3.0% to ~3.3%, whereas the composite with the PARC matrix exhibited increased porosity, ranging from ~4.5% to ~4.8%.

3. Pre-testing Morphology of Composites

3.1. WCM: Baseline Composite vs. the Composite with PARC Matrix

Optical micrographs at two different magnifications for both the baseline composite and the composite with the PARC matrix, fabricated using vacuum-assisted WCM method, are presented in Figures 6-7. As shown in Figure 5, the fabrics were well impregnated with the baseline matrix, exhibiting minimal voids in the composite, as confirmed by the measured void volume fraction of ~1.2 to ~1.4%.

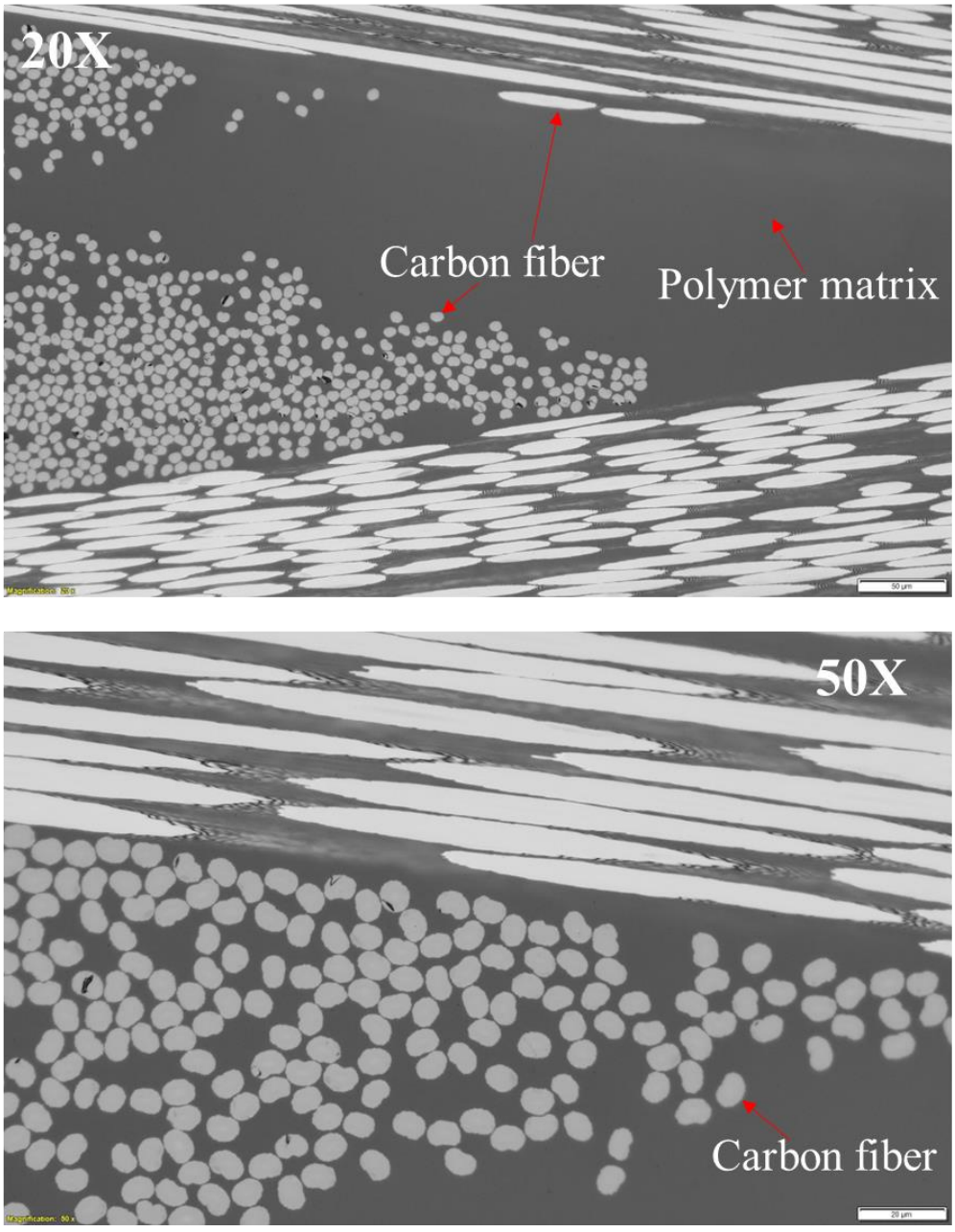

Figure 6. Micrographs of baseline fiber-reinforced composite fabricated by WCM.

In contrast, as shown in Figure 7 for the composite with the PARC matrix fabricated using vacuum-assisted WCM method, recycled CFRP particles ranging in size from ~0.2 μm to ~5 μm were uniformly distributed between the fibers and throughout the composite. Although voids are present at various locations within the composite, they are not significant, which is consistent with the measured void volume fraction of approximately 2.1% to 2.4%.

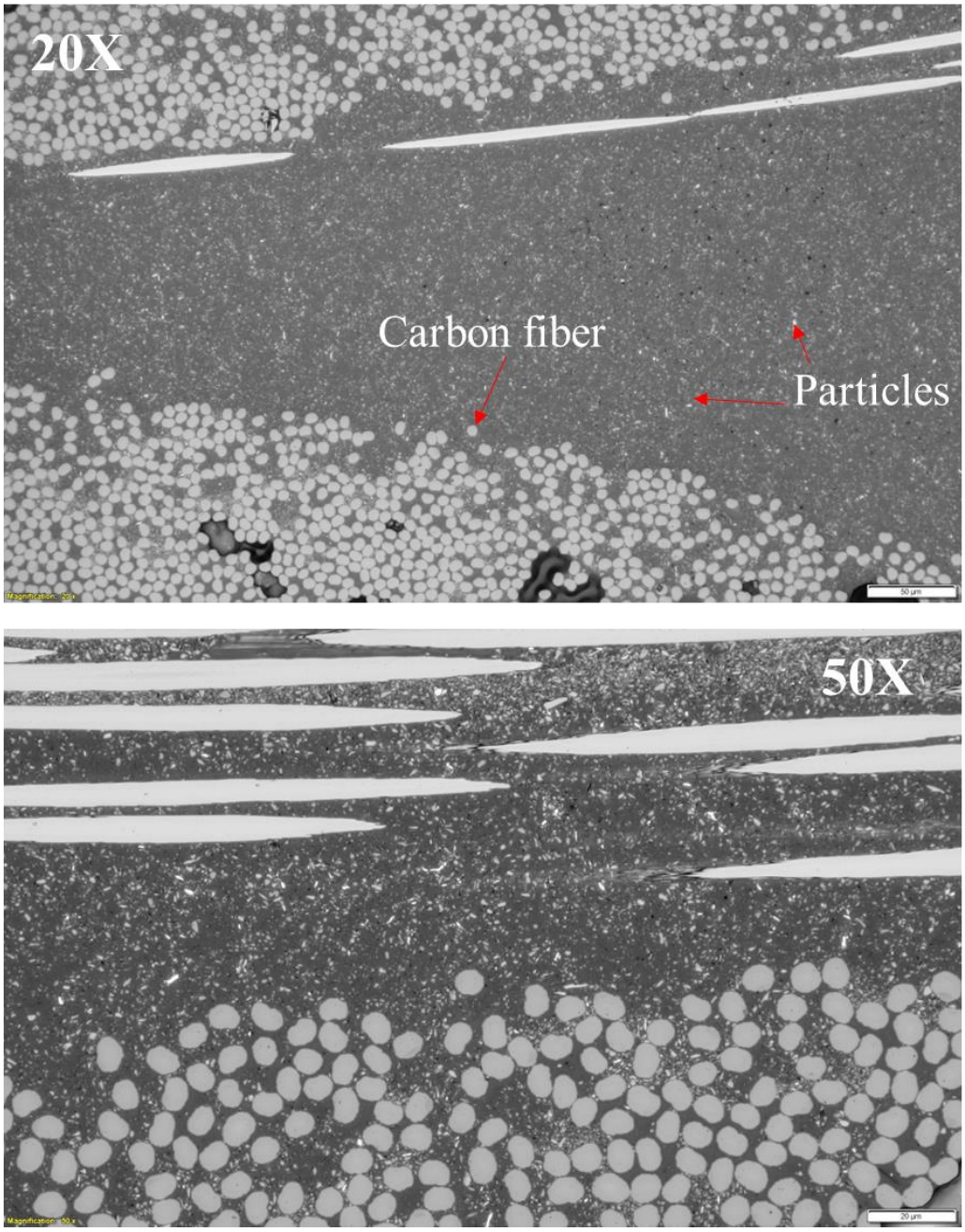

Figure 7. Micrographs of the fiber-reinforced composite with PARC matrix fabricated by WCM.

3.2. Filament Winding: Baseline Composite vs. the Composite with PARC Matrix

Optical micrographs at two different magnifications of both the baseline composite and the composite with the PARC matrix, fabricated using wet filament winding, are presented in Figure 8. As shown, the fabrics were well impregnated with both matrices; however, noticeable voids are present in the composites, confirming the higher void volume fractions measured in these composites compared to those fabricated using WCM. This aspect can be attributed to the winding processing parameters, such as winding speed and matrix dripping during the winding process.

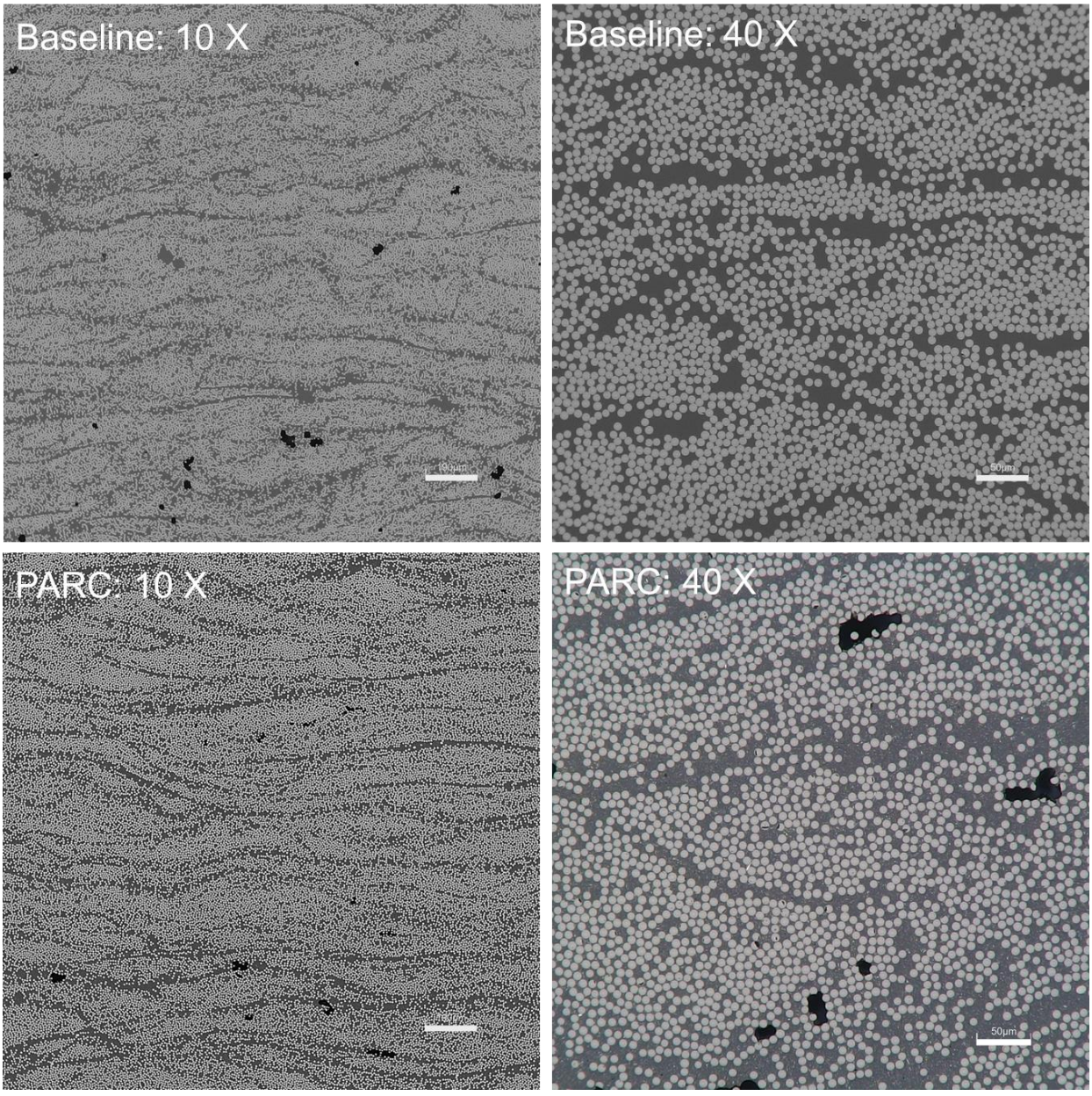

Figure 8. Micrographs of the fiber-reinforced composites fabricated by wet filament winding.

4. Thermal and Mechanical Behaviors

4.1. Thermal Behavior of Matrix

As shown in Figure 9, the CTE values of both matrices display two distinct stages across the investigated temperature range. The T_g value can be identified at the intersection of the two slopes, as demonstrated in Figure 9. The T_g value of the PARC matrix was approximately 10℃ lower than that of the baseline matrix. Moreover, the PARC matrix exhibits consistently 20% lower CTE values across the investigated temperatures compared to the baseline matrix. The foregoing changes in thermal behavior caused by the addition of recycled CFRP particles to the epoxy matrix can reduce thermal deformation.

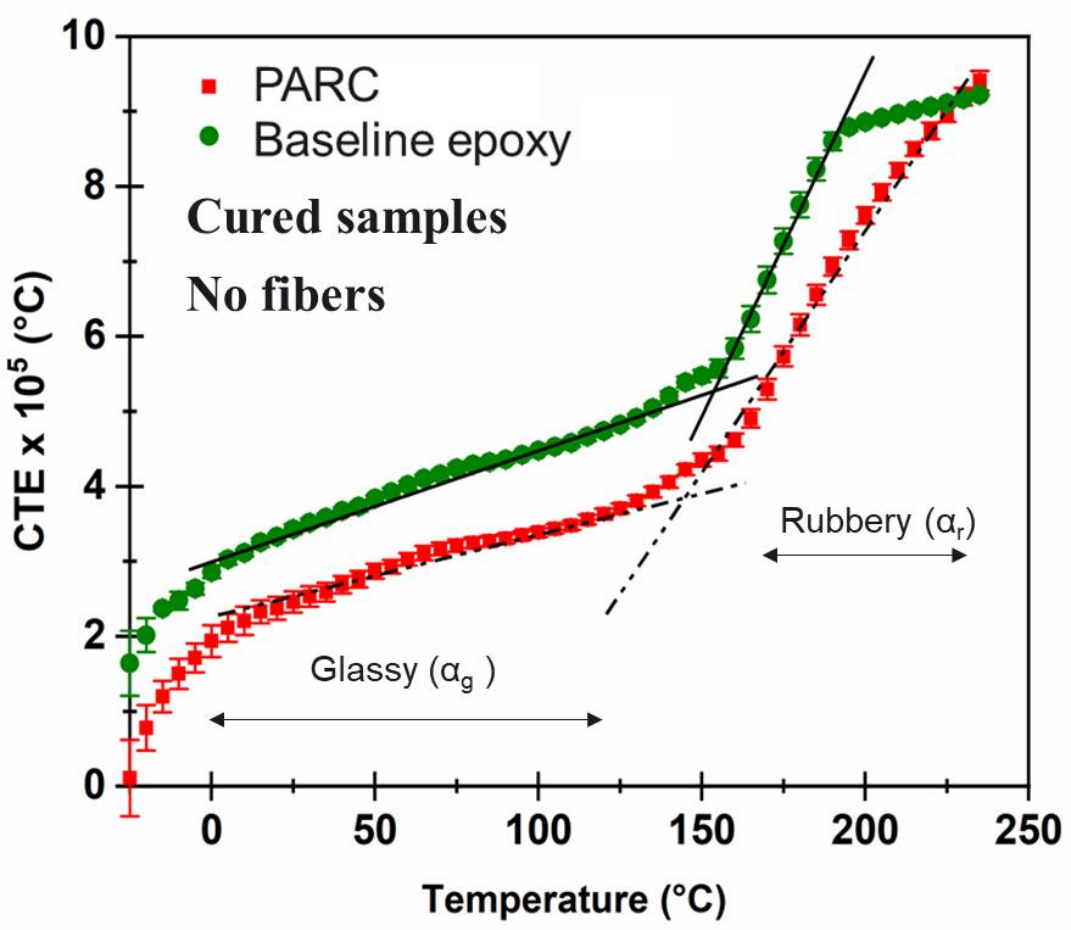

Figure 9. CTE values as a function of temperature for both the baseline and PARC matrices.

On the other hand, the heat flow as a function of heating temperature for three different heating rates, as shown in Figure 10, highlights the differences in curing kinetics between the baseline and PARC matrices. As it can be seen from this figure, PARC matrix starts to cure early than that of baseline matrix. This aspect can be attributed to the improved thermal conductivity resulting from the addition of recycled CFRP particles, as evidenced by the lower activation energy barrier of the PARC matrix (86 kJ/mol) compared to the baseline matrix (140 kJ/mol). Despite these differences, the total curing times for the baseline and PARC matrices were very

similar, with the PARC matrix curing approximately 2 minutes slower, likely due to the more uniform temperature distribution induced by the enhanced thermal conductivity.

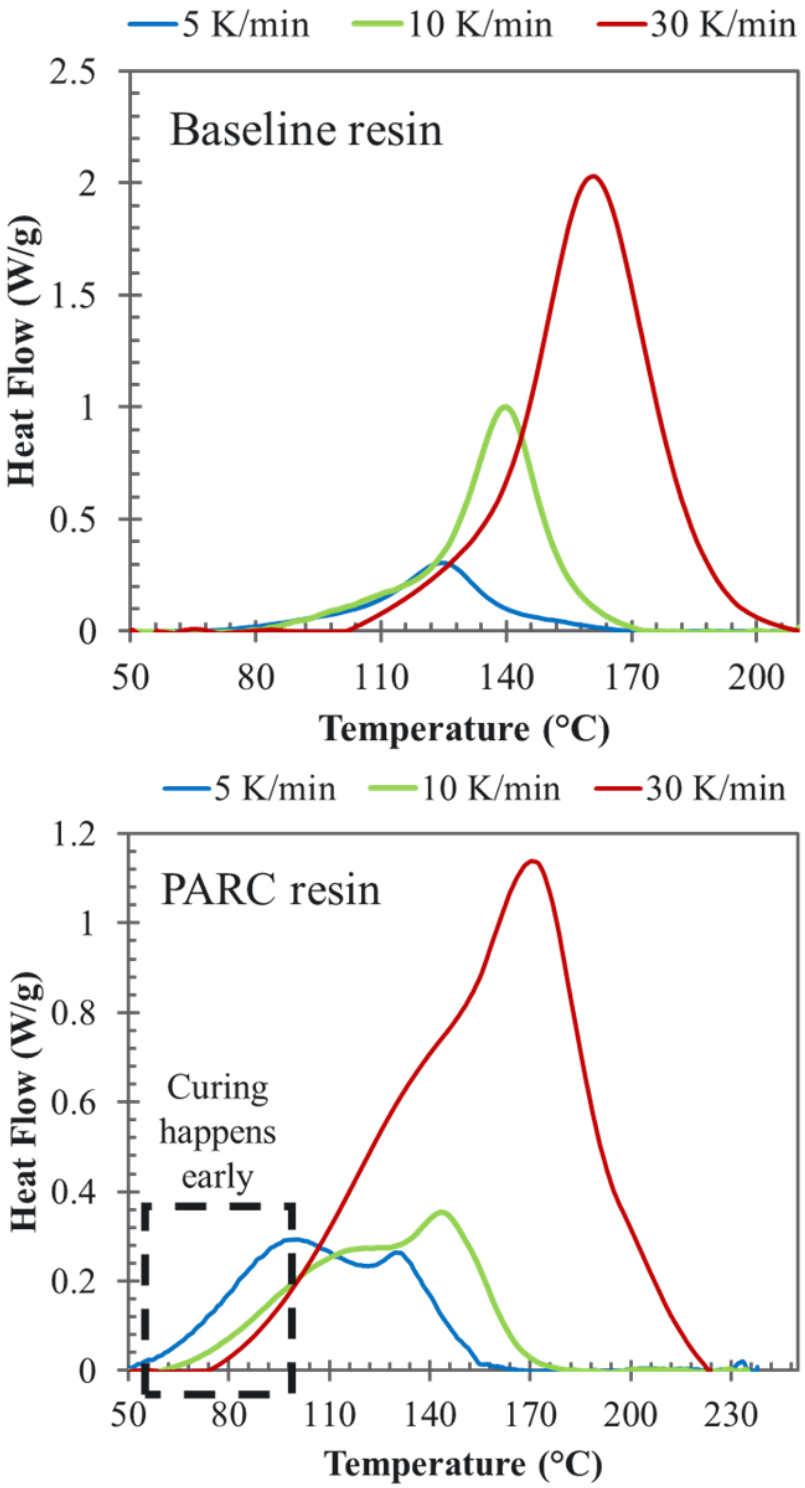

Figure 10. Heat flow as a function of temperature using three different heating rates for both the baseline and PARC matrices.

4.2. Uni-axial Tension and Flexure of Composites

In uni-axial tension (Figure 11), the composite with the PARC matrix exhibits a higher average tensile strength and elastic modulus (478 MPa) compared to the baseline matrix (448 MPa) when fabricated using the traditional WCM method. However, the elastic modulus of both composites exhibited very similar values (~43 GPa) as shown in Figure 11. The improvement on tensile strength can be attributed to the enhanced fracture energy of the matrix due to the addition of recycled CFRP particles [2,3]. It is worth mentioning here that the failure of composites happened within the gauge area as shown in Figure 11.

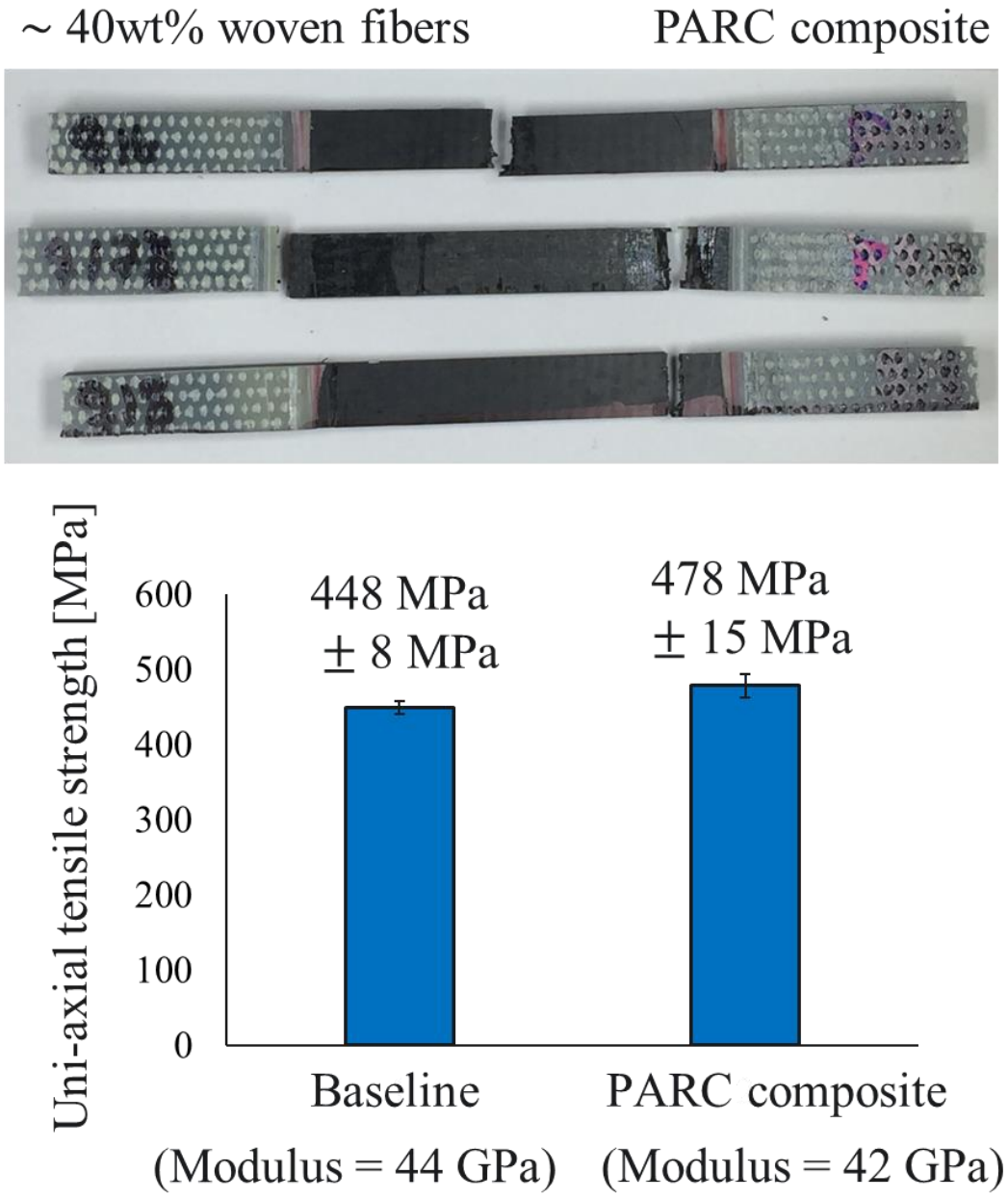

Figure 11. Comparison on uni-axial tensile strength and elastic modulus between the composites with baseline and PARC matrices. Failure of the composite with PARC matrix was also shown as an example.

In four-point bending (Figure 12), when comparing the traditional and vacuum-assisted WCM methods, the flexural strength with the highest probability for the composite with the PARC matrix shows no significant difference. However, the vacuum-assisted WCM method reduced the scattering of the flexural strength range compared to the traditional WCM method, as shown in Figure 12.

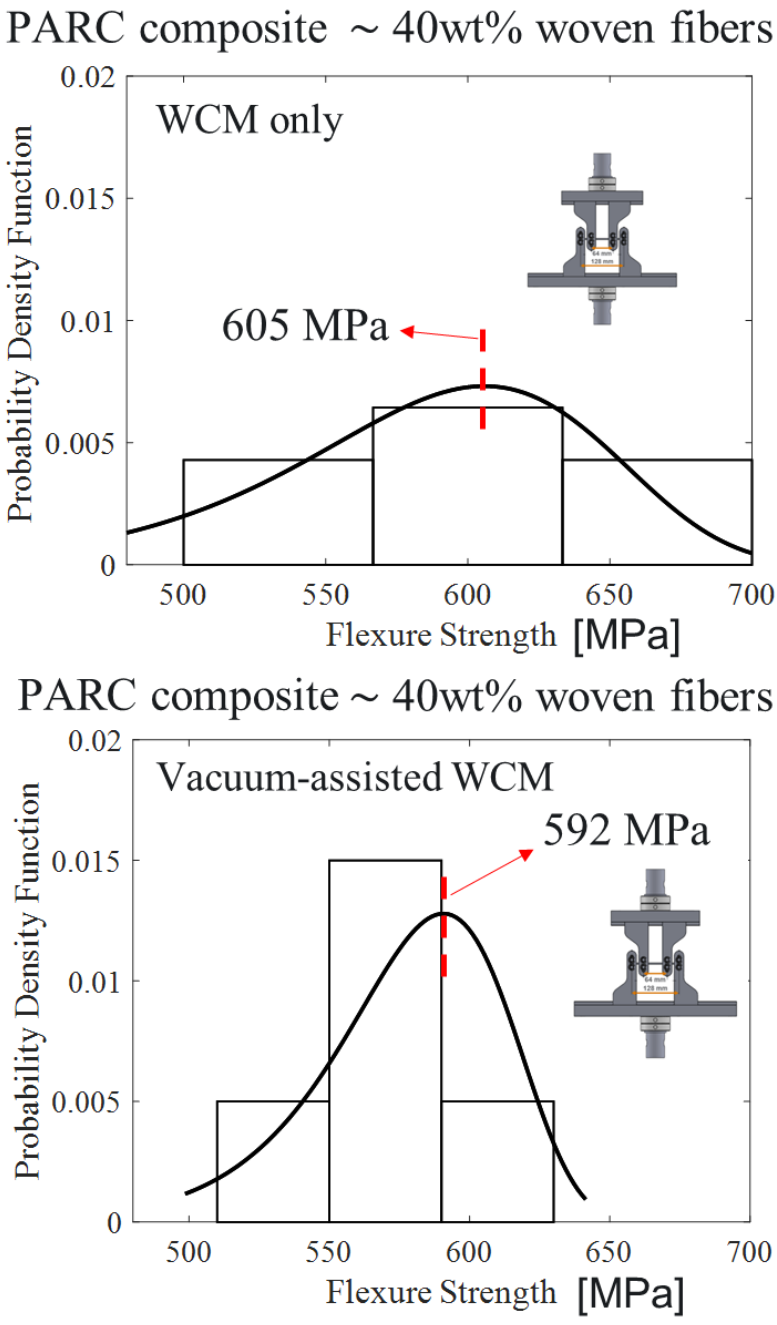

Figure 12. Probability density function of flexure strength of the composites with PARC matrix. This figure compares the difference between traditional and vacuum-assisted WCM methods.

On the other hand, as shown in Figures 13-14 for the case of vacuum-assisted WCM method, both the flexural strength and elastic modulus, at their highest probabilities, can be improved by approximately 10% by incorporating recycled CFRP particles into the baseline matrix to form the PARC matrix in the composite. The elastic modulus with the most probability was improved from 41 GPa to 44 GPa, whereas the flexure strength with the most probability was improved from 580 MPa to 612 MPa.

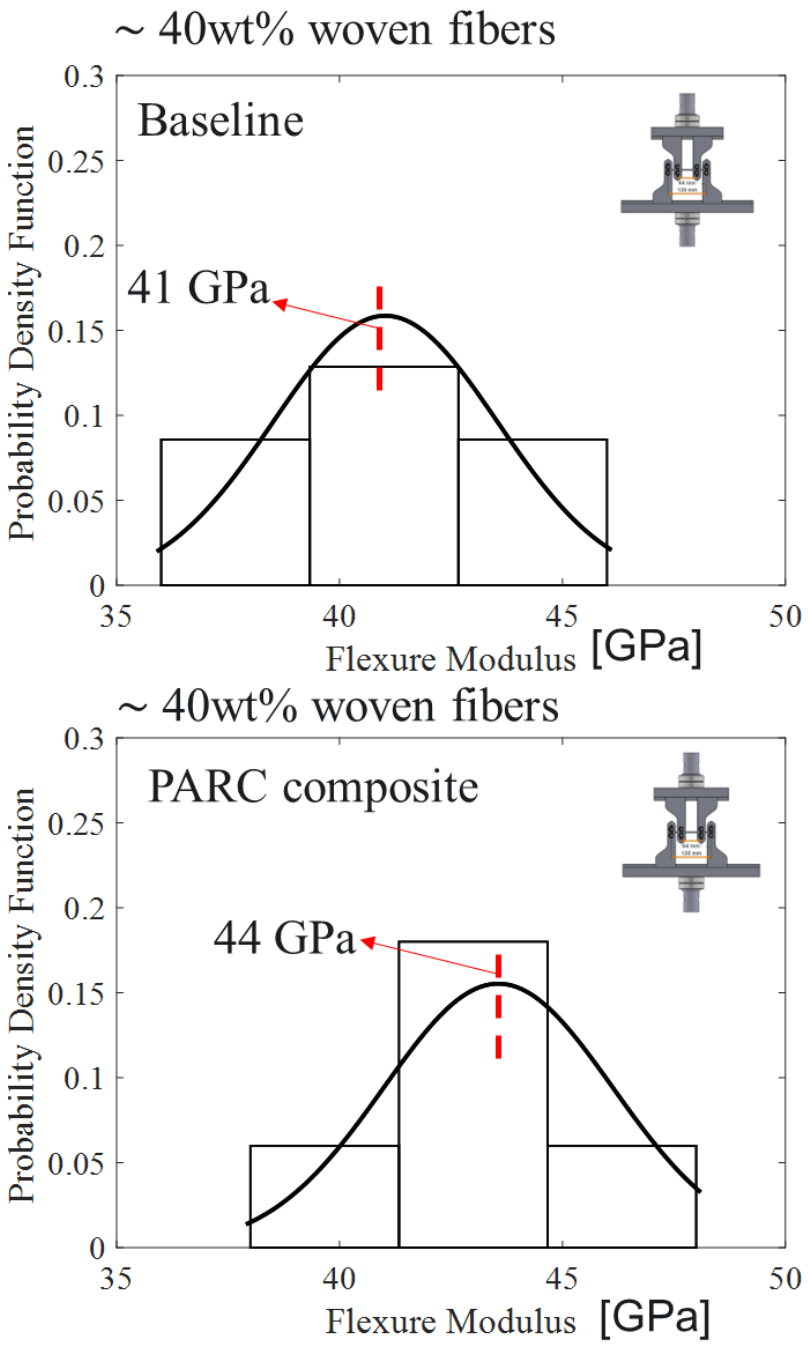

Figure 13. Probability density function of flexure modulus of the composites with baseline and PARC matrices.

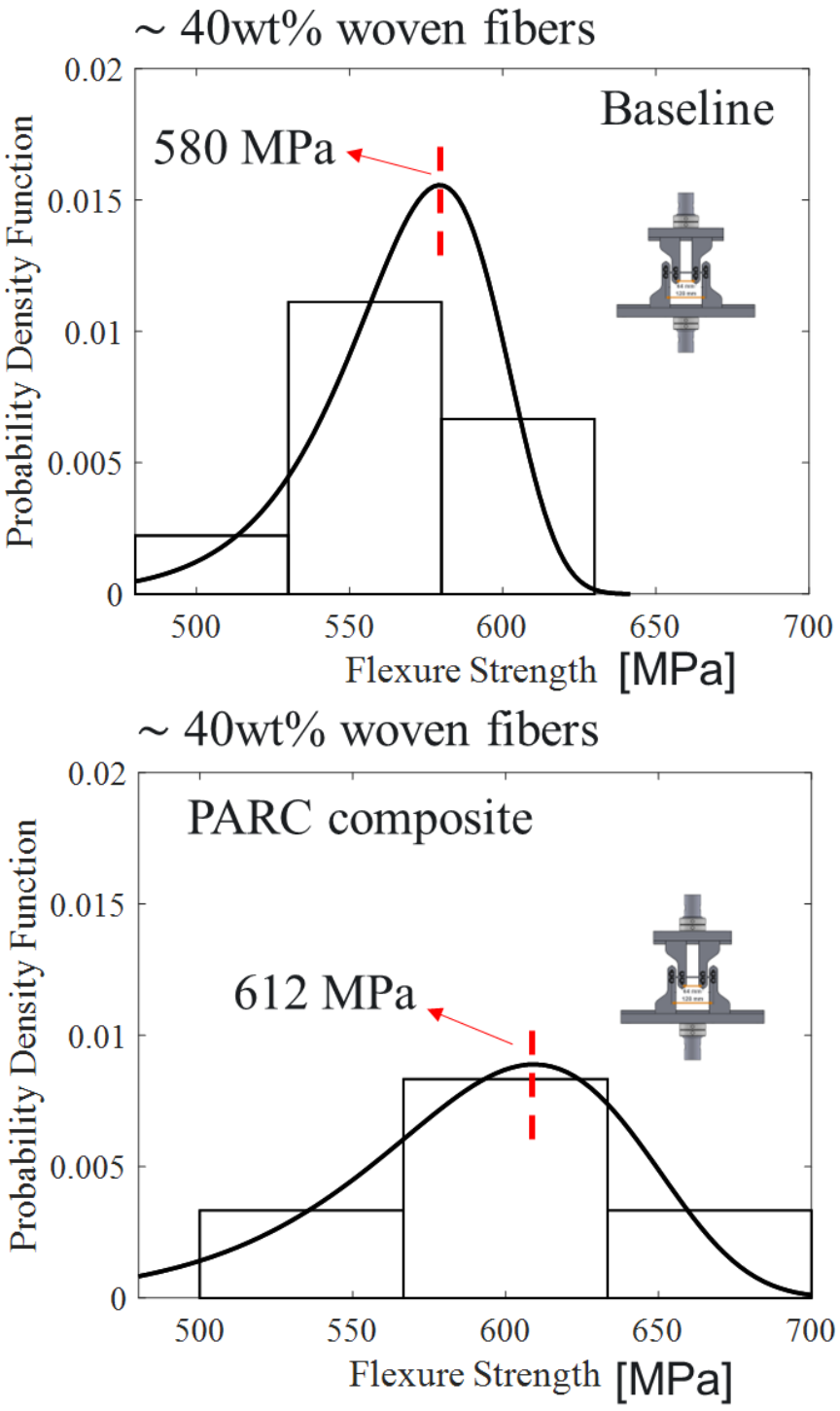

Figure 14. Probability density function of flexure strength of the composites with baseline and PARC matrices.

4.3. Interlaminar Shear Strength of Composites

The interlaminar shear strength of curved composites cut from filament-wound composite rings was also measured and plotted in Figure 15. As shown in the figure, the interlaminar shear strength of the composites with either the baseline or PARC matrix does not exhibit a significant difference, both being approximately 67 MPa to 70 MPa. However, their damage morphologies exhibit a noticeable difference as shown in Figures 16-17. The composite with the PARC matrix exhibits more delamination (i.e., interlaminar cracks) compared to the baseline matrix at the same displacement of approximately 1.25 mm. This phenomenon can be attributed to defects such as voids and agglomeration introduced by the addition of recycled CFRP particles, which lead to higher stress concentrations and facilitate delamination. Although the specimens were not loaded until the load dropped to zero, the composite with the PARC matrix can reasonably exhibit higher toughness due to greater energy dissipation from increased delamination.

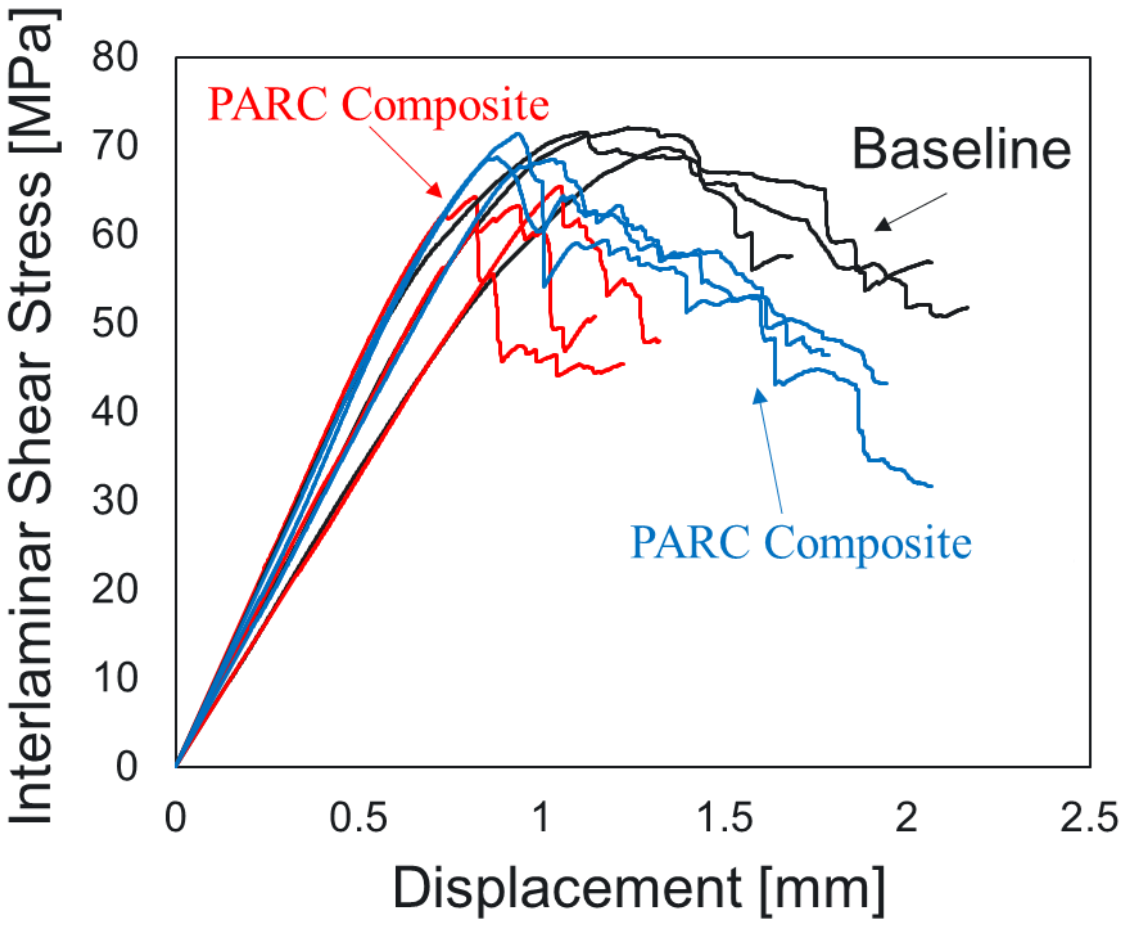

Figure 15. Interlaminar shear stress versus displacement for the curved composites with baseline and PARC matrices.

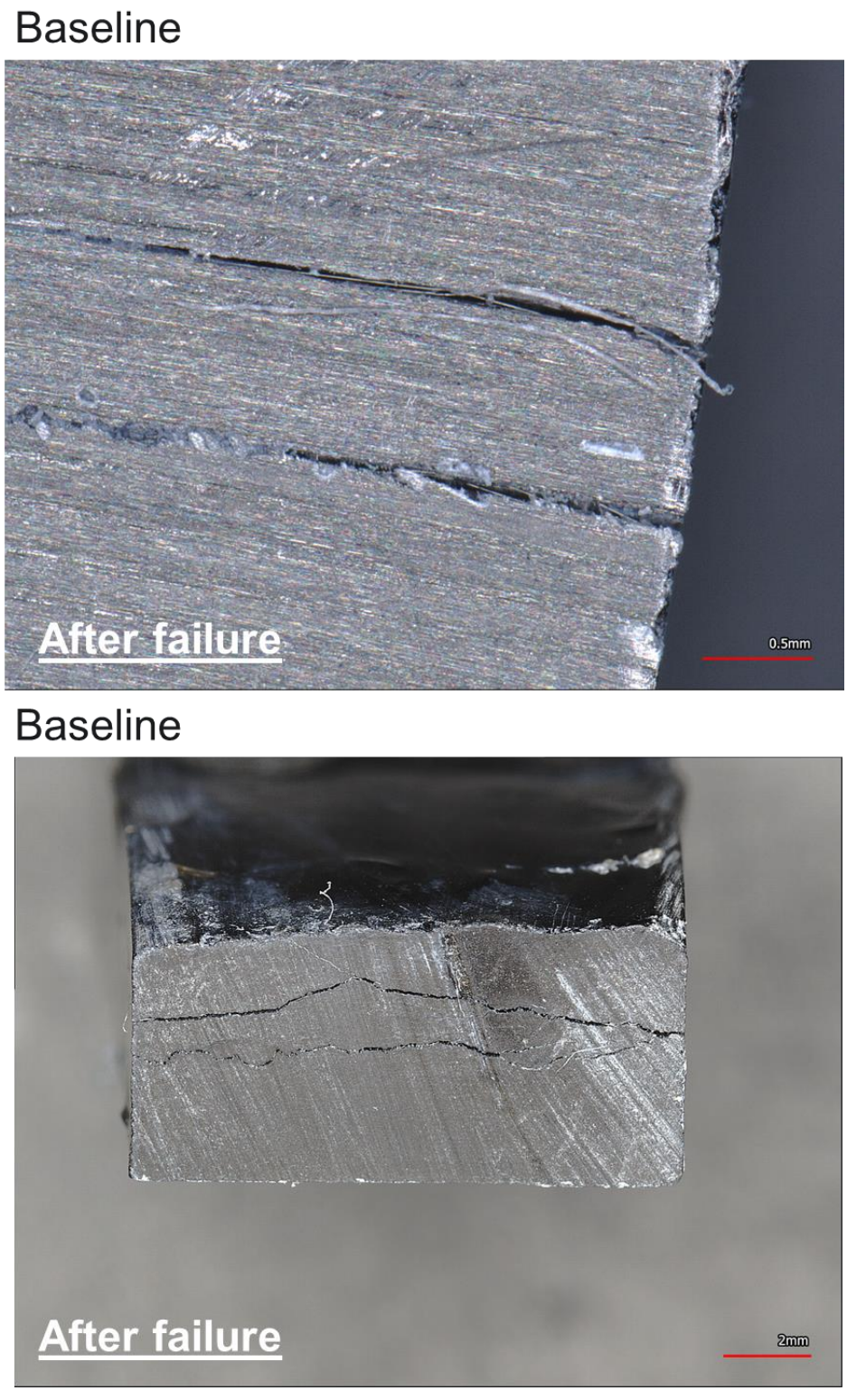

Figure 16. Damage morphology of the curved composite with baseline matrix under short-beam shear testing. The specimen was removed from the testing machine at the displacement of ~1.25 mm.

Figure 17. Damage morphology of the curved composite with PARC matrix under short-beam shear testing. The specimen was removed from the testing machine at the displacement of ~1.25 mm.

5. Conclusions

Based on the results obtained from this project, the following conclusions can be summarized:

1. Both vacuum-assisted wet compression molding and wet filament winding methods have been developed for fabricating fiber-reinforced composites with the PARC matrix;

2. The PARC matrix exhibited a ~10℃ lower glass transition temperature and 20% lower coefficient of thermal expansion values compared to the baseline matrix across the investigated temperatures (room temperature to 200℃);

3. The PARC matrix exhibited earlier curing initiation and a lower activation energy barrier (86 vs. 140 kJ/mol) due to improved thermal conductivity from recycled CFRP particles;

4. Composites with the PARC matrix exhibited higher porosity compared to baseline composites, with increases of ~1% for WCM and ~1.5% for filament winding methods;

5. Composites with the PARC matrix fabricated via WCM showed ~10% higher uniaxial tensile and four-point bending strengths and moduli compared to baseline composites;

6. Filament-wound composites with baseline and PARC matrices exhibited similar interlaminar shear strength, though potential toughness improvements with the PARC matrix require further investigation.

References

1. Iftime G, Wei J, Pandey R, Garner SR. Recyclable enhanced performance carbon fiber reinforced polymers, 2021, Application number: 17080998

2. Mefford CH, Qiao Y, Salviato M. Failure Behavior and Scaling of Graphene Nanocomposites. Compos Struct 2017;176:961-72.

3. Qiao Y, Salviato M. Study of the Fracturing Behavior of Thermoset Polymer Nanocomposites via Cohesive Zone Modeling. Compos Struct 2019;220:127-47.

Acknowledgements

We would like to acknowledge Lisa D. Fring, Madhusudhan R. Pallaka, Ethan K. Nickerson, and Rob J. Seffens of Pacific Northwest National Laboratory for helping the mechanical and thermal testing. We also thank Gabriel Iftime, Austin Wei, and Rahul Pandey for providing the PARC matrix and for their contributions to research discussions.

This work is supported by the U.S. Department of Energy, Office of Energy Efficiency and Renewable Energy, Vehicle Technologies Office, LightMAT (Lightweight Materials Consortium). PNNL is operated by Battelle Memorial Institute for the U.S. Department of Energy under contract DE-AC06-76RLO 1830.

Pacific Northwest National Laboratory

902 Battelle Boulevard
P.O. Box 999
Richland, WA 99354
1-888-375-PNNL (7665)

www.pnnl.gov